

Pure hyperfine spectra of KRb in its vibronic ground state: Towards the determination of nuclear spin-spin interaction

Qi Ouyang(欧阳琪), Xu-Ping Shao(邵旭萍), Yun-Xia Huang(黄云霞), and Xiao-Hua Yang(杨晓华)
Citation: Chin. Phys. B, 2025, 34 (**5**): 053302. DOI: 10.1088/1674-1056/adbdc1
http://cpb.iphy.ac.cn; http://iopscience.iop.org/cpb

What follows is a list of articles you may be interested in

Spectroscopic study of $B^2\Sigma^+$–$X_1\ ^2\Pi_{1/2}$ transition of electron electric dipole moment candidate PbF

Ben Chen(陈犇), Yi-Ni Chen(陈旖旎), Jia-Nuan Pan(潘佳煖), Jian-Ping Yin(印建平), and Hai-Ling Wang(汪海玲)†
Chin. Phys. B, 2022, 31 (**9**): 093301. DOI: 10.1088/1674-1056/ac633a

Laser-induced fluorescence experimental spectroscopy and theoretical calculations of uranium monoxide

Xi-Lin Bai(白西林), Xue-Dong Zhang(张雪东), Fu-Qiang Zhang(张富强), and Timothy C Steimle
Chin. Phys. B, 2022, 31 (**5**): 053301. DOI: 10.1088/1674-1056/ac43a4

Compton profile of molecular hydrogen

Zhao Xiao-Li (赵小利), Yang Ke (杨科), Xu Long-Quan (徐龙泉), Ma Yong-Peng (马永朋), Yan Shuai (闫帅), Ni Dong-Dong (倪冬冬), Kang Xu (康旭), Liu Ya-Wei (刘亚伟), Zhu Lin-Fan (朱林繁)
Chin. Phys. B, 2015, 24 (**3**): 033301. DOI: 10.1088/1674-1056/24/3/033301

Autler–Townes splitting in photoelectron spectra of K_2 molecule

Yao Hong-Bin(姚洪斌) and Zheng Yu-Jun(郑雨军)
Chin. Phys. B, 2012, 21 (**2**): 023302. DOI: 10.1088/1674-1056/21/2/023302

Pure hyperfine spectra of KRb in its vibronic ground state: Towards the determination of nuclear spin–spin interaction

Qi Ouyang(欧阳琪), Xu-Ping Shao(邵旭萍)[†], Yun-Xia Huang(黄云霞), and Xiao-Hua Yang(杨晓华)[‡]

School of Physical Science and Technology, Nantong University, Nantong 226019, *China*

(Received 16 January 2025; revised manuscript received 23 February 2025; accepted manuscript online 7 March 2025)

The Zeeman-hyperfine-rotational spectra of ^{40}K^{87}Rb within its vibronic ground state at a magnetic field of 545.9 G are investigated by adopting the latest molecular constants available, and the results are in good agreement with the experimental observation made by Ospelkaus *et al.* [*Phys. Rev. Lett.* **104** 030402 (2010)]. However, the calculated spectra generally shift by −3.6 kHz from the experimental ones, which implies the inaccuracy of the effective rotational constant. Therefore, we refit the spectra and obtain a new $B_{\rm eff} = 1113952(1)$ kHz, which reduces the overall root-mean-square deviation from 10.8 kHz to 7.9 kHz. Furthermore, the pure hyperfine spectra within the $J = 0$ and 1 rotational states are simulated. We find that the scalar nuclear spin–spin interaction dominates the hyperfine splitting of $J = 0$ despite it being slightly indirectly affected by the nuclear electric quadruple interaction due to the rotational perturbation, while the nuclear electric quadrupole interactions dominate the splitting, and the scalar and tensor nuclear spin–spin interactions also affect the splitting of $J = 1$. The detailed hyperfine-rotational perturbations are studied. Therefore, the scalar and tensor nuclear spin–spin interaction constants can be precisely determined by simultaneously measuring the pure hyperfine radio-frequency spectra of the $J = 0$ and 1 states in the vibronic ground state.

Keywords: pure hyperfine spectrum, transition dipole moment, ^{40}K^{87}Rb

PACS: 33.20.Bx, 33.70.Ca, 33.25.+k, 33.15.Pw

DOI: 10.1088/1674-1056/adbdc1 **CSTR:** 32038.14.CPB.adbdc1

1. Introduction

Cold molecular physics has been at the forefront of atomic, molecular and optical physics for over two decades due to its unprecedented applications in many related fields, such as quantum information,[1] quantum computation,[2,3] cold chemistry,[4] precision spectroscopy and precision measurements.[5,6] However, the molecular structures are very complicated compared to those of atoms, which makes it an outstanding experimental challenge to reach molecular quantum Fermi degeneracy or Bose–Einstein condensation (BEC).

Ultracold (≤ 1 μK) molecules can be achieved by direct laser-cooling of molecules, such as SrF,[7] YO,[8] CaF[9] and BaF,[10] with highly diagonal Franck–Condon factors and coherent adiabatic association of laser-cooled deeply degenerate mixture of alkali atoms.[11–16] The alkali polar molecules are the coldest achieved species and they have reached the Fermi degenerate[17,18] or BEC[19] regime. Such low temperature cancels out all the broadening effects except the natural ones, which produces precision spectroscopy. Thus, weak intramolecular interactions can be observed and precise physical constants can be determined, which may be applied in searching the electron's electric dipole moment (eEDM)[20,21] and in testing possible time-variation of the fine-structure constant α.[22] The molecular nuclear spin–spin interaction can also be precisely determined, which may affect the chemical reaction in the cold regime.[23] The precise spectroscopy determined molecular hyperfine structures help us to investigate cold molecular interactions and even to further cool cold molecules to the quantum regime.

In addition to breakthroughs in the achievement of ultracold alkali polar molecules, studies on the hyperfine-rotational spectroscopy of KRb have also been fruitful, both theoretically[24–26] and experimentally.[27] Aldegunde *et al.* calculated the nuclear quadrupole and magnetic coupling constants for ^{39}K^{85}Rb by employing density-functional theory and explored the hyperfine structures in the applied fields in 2008.[24] They calculated the hyperfine-rotational spectra in the $J = 1 \leftarrow 0$ transition within the vibronic ground state of ^{40}K^{87}Rb in the presence of electric and magnetic fields in 2009.[25] Ran *et al.* further calculated the hyperfine-rotational spectra of ^{41}K^{87}Rb in mixed electric and magnetic fields in 2010.[26] Microwave hyperfine-rotational spectra were observed and analyzed by Ye's group in the same year.[27]

In the present study, the hyperfine structures of ^{40}K^{87}Rb molecules in the vibronic ground state are theoretically studied in both the coupled and uncoupled basis sets, and the results are compared with the experimental ones.[27] The transition dipole moment is deduced, and thus, the transition selection rules are summarized. As a result, the pure hyperfine, radio-frequency (RF) spectra within the vibronic ground state

[†]Corresponding author. E-mail: xuping1115@ntu.edu.cn

[‡]Corresponding author. E-mail: xhyang@ntu.edu.cn

© 2025 Chinese Physical Society and IOP Publishing Ltd. All rights, including for text and data mining, AI training, and similar technologies, are reserved.

of KRb can be predicted. The weak hyperfine perturbation and rotational perturbation are discussed as well.

2. Theory

The hyperfine-rotational Hamiltonian consists of the rotational ($H_{\rm rot}$) and hyperfine ($H_{\rm hf}$) terms. The values of the electronic and vibrational terms can be set at zero when studying the vibronic ground state. However, even if we only study the rotational ground state, the rotational terms must be included due to the rotational perturbation. The rotational term is of the well-known form, and the hyperfine consists of three parts: the nuclear electric quadrupole interactions with the gradient of the electric field produced by the electrons surrounding $H_{\rm Q} = -e\sum_{i=1,2} T^{(2)}(Q_i)\cdot T^{(2)}(\nabla E_i)$, the nuclear spin–rotational interaction $H_{\rm sr} = C_1 \boldsymbol{J}\cdot\boldsymbol{I}_1 + C_2 \boldsymbol{J}\cdot\boldsymbol{I}_2$ and the nuclear spin–spin interaction $H_{\rm ss} = C_3 \boldsymbol{I}_1\cdot T\cdot \boldsymbol{I}_2 + C_4 \boldsymbol{I}_1\cdot\boldsymbol{I}_2$. Here, e is the charge of an electron, Q_i is the nuclear electric quadrupole moment and $i = 1$ or 2 denotes the two atoms forming the molecule, ∇E_i is the gradient of the electric field produced by the electrons at the nuclei, $T^{(2)}(x)$ is the second-rank tensor, C_1 and C_2 are the nuclear spin–rotation coupling constants, and C_3 and C_4 are the nuclear spin–spin coupling tensor and scalar constants, respectively.

The coupled basis is represented as $|\boldsymbol{J}\boldsymbol{I}_1\boldsymbol{G}\boldsymbol{I}_2\boldsymbol{F}\rangle$, where $\boldsymbol{J}$ is the molecular total angular momentum excluding the nuclear spin, $\boldsymbol{I}_1$ and $\boldsymbol{I}_2$ are the respective nuclear spins of the two atoms, $\boldsymbol{G}$ is the intermediate angular moment of $\boldsymbol{J}$ coupling with the larger nuclear spin ($\boldsymbol{I}_1$) and $\boldsymbol{F}$ is the molecular total angular momentum of $\boldsymbol{G}$ coupling with $\boldsymbol{I}_2$. For the ^{40}K^{87}Rb molecule, the nuclear spins of ^{40}K and ^{87}Rb are 4 and 3/2, respectively. The detailed Hamiltonian matrix of the hyperfine-rotational structure can be found in Ref. [28] and deduced on the basis of $|\boldsymbol{J}\boldsymbol{I}_1\boldsymbol{G}\boldsymbol{I}_2\boldsymbol{F}\rangle$ as follows:

$$\begin{aligned}
&\langle J',I_1,G',I_2,F'|H_{\rm rot}|J,I_1,G,I_2,F\rangle\\
&= B_v J(J+1) - D_v J^2(J+1)^2, \qquad (1)\\
&\langle J',I_1,G',I_2,F'|H_{\rm sr}|J,I_1,G,I_2,F\rangle\\
&= C_1(-1)^{J+J'+I_1+I_2+F'+G+1}[(2F+1)(2F'+1)(2G+1)]^{1/2}\\
&\times[(2J+1)(J+1)J(2I_1+1)(I_1+1)I_1]^{1/2}\\
&\times\begin{Bmatrix} G' & F' & I_2\\ F & G & 1\end{Bmatrix}\begin{Bmatrix} J' & I_1 & G\\ I_1 & J & 1\end{Bmatrix}\\
&+C_2(-1)^{J+I_1+I_2+F+2G'+1}[(2F+1)(2G'+1)(2G+1)]^{\frac{1}{2}}\\
&\times[(2J+1)(J+1)J(2I_2+1)(I_2+1)I_2]^{\frac{1}{2}}\\
&\times\begin{Bmatrix} G' & I_2 & F\\ I_2 & G & 1\end{Bmatrix}\begin{Bmatrix} J' & G' & I_1\\ G & J & 1\end{Bmatrix}, \qquad (2)\\
&\langle J',I_1,G',I_2,F'|H_{\rm ss}|J,I_1,G,I_2,F\rangle\\
&= C_3(-1)^{J+I_2+F+G'}[30(2G+1)(2G'+1)(2J+1)(2J'+1)]^{\frac{1}{2}}\\
&\times[(2I_2+1)(I_2+1)I_2(2I_1+1)(I_1+1)I_1]^{\frac{1}{2}}\\
&\times\begin{pmatrix} J & 2 & J'\\ 0 & 0 & 0\end{pmatrix}\begin{Bmatrix} I_2 & G' & F\\ G & I_2 & 1\end{Bmatrix}\begin{Bmatrix} J & J' & 2\\ I_1 & I_1 & 1\\ G & G' & 1\end{Bmatrix}\\
&+C_4(-1)^{J+I_1+I_2+F+G+G'+1}[(2G+1)(2G'+1)]^{1/2}\\
&\times[(2I_2+1)(I_2+1)I_2(2I_1+1)(I_1+1)I_1]^{\frac{1}{2}}\\
&\times\begin{Bmatrix} I_2 & G' & F\\ G & I_2 & 1\end{Bmatrix}\begin{Bmatrix} G & I_1 & J\\ I_1 & G' & 1\end{Bmatrix}, \qquad (3)\\
&\langle J',I_1,G',I_2,F'|H_{\rm Q}|J,I_1,G,I_2,F\rangle\\
&= \frac{1}{4}eQq_1(-1)^{I_1+2J'+G}[(2J+1)(2J'+1)]^{\frac{1}{2}}\\
&\times\begin{Bmatrix} G & J' & I_1\\ 2 & I_1 & J\end{Bmatrix}\begin{pmatrix} J' & 2 & J\\ 0 & 0 & 0\end{pmatrix}\begin{pmatrix} I_1 & 2 & I_1\\ -I_1 & 0 & I_1\end{pmatrix}^{-1}\\
&+\frac{1}{4}eQq_2(-1)^{I_1+I_2+F+G+J+J'+G'}\\
&\times[(2J+1)(2J'+1)(2G+1)(2G'+1)]^{\frac{1}{2}}\begin{Bmatrix} F & I_2 & G'\\ 2 & G & I_2\end{Bmatrix}\\
&\times\begin{Bmatrix} I_1 & G' & J'\\ 2 & J & G\end{Bmatrix}\begin{pmatrix} J' & 2 & J\\ 0 & 0 & 0\end{pmatrix}\begin{pmatrix} I_2 & 2 & I_2\\ -I_2 & 0 & I_2\end{pmatrix}^{-1}, \qquad (4)
\end{aligned}$$

where B_v and D_v are the rotational and centrifugal distortion constants, eQq_i represents the nuclear electric quadrupole constant, and ( ) and { } are the Wigner 3-j and 6-j symbols, respectively.

The molecular pure hyperfine spectrum originates from the magnetic dipole transition. The nuclear transition moments of the magnetic dipole on the basis of $|\boldsymbol{J}\boldsymbol{I}_1\boldsymbol{G}\boldsymbol{I}_2\boldsymbol{F}\rangle$ are expressed as follows:

$$\begin{aligned}
d_{m_1} &= g_1\mu_{\rm N}(-1)^{G+F'+I_2}\sqrt{(2F+1)(2F'+1)}\\
&\times\begin{Bmatrix} G & F & I_2\\ F' & G' & 1\end{Bmatrix}\begin{Bmatrix} I_1 & G & J\\ G' & I_1 & 1\end{Bmatrix}\\
&\times(-1)^{J+G+I_1}\\
&\times\sqrt{(2G+1)(2G'+1)I_1(I_1+1)(2I_1+1)}, \qquad (5)\\
d_{m_2} &= g_2\mu_{\rm N}(-1)^{G+F+I_2+1}\\
&\times\sqrt{(2F+1)(2F'+1)I_2(I_2+1)(2I_2+1)}\\
&\times\begin{Bmatrix} I_2 & F & G\\ F' & I_2 & 1\end{Bmatrix}, \qquad (6)
\end{aligned}$$

where g_i is the nuclear g-factor and $\mu_{\rm N}$ is the nuclear magneton. Therefore, the total transition magnetic moment is the sum of the above two equations, and the spectral intensities are proportional to its square. Thus, the pure hyperfine spectral transition selection rule is $\Delta F = 1$.

3. Results and discussion

3.1. Zeeman-hyperfine-rotational spectra of $J = 1 \leftarrow 0$ at $B = 545.9$ G

The presence of a magnetic field may destroy the conservation of F, in which case only the total projection quantum number M_F is conserved. The Zeeman-hyperfine-rotational

spectra of ^{40}K^{87}Rb of the $J = 1 \leftarrow 0$ transition within its vibronic ground state ($X^1\Sigma$, $v = 0$) are calculated on both the coupled $|JI_1GI_2FM_F\rangle$ and uncoupled basis set $|JM_JM_1M_2\rangle$, where M_J, M_1 and M_2 are the projections of J, I_1 and I_2 onto the Z-axis defined by the direction of the field. The connection of the quantum numbers between the coupled and uncoupled basis sets in the low-J case is as follows: $G = I_1 + M_J$, $F = G + M_2$ and $M_F = M_J + M_1 + M_2$. The molecular constants adopted in the present study are from Ref. [24] and listed in Table 1. The relative errors of the two methods are within 10^{-5} at an applied magnetic field of 545.9 G, as listed in columns 6 and 7 of Table 2. However, the uncoupled one achieves more accurate results due to the decoupling of the molecular angular momenta as the magnetic field is increasing. Therefore, the spectra at the applied magnetic field are calculated on the uncoupled basis, while the field-free spectra are calculated on the coupled basis in the next two subsections. The electric dipole transition is allowed between states with opposite parity, while the magnetic dipole transition is allowed between states with the same parity. The spectrum is usually caused by either electric or magnetic dipole transition. However, the electric and the magnetic dipole transitions may occur simultaneously when a state is composed of states with opposite parity due to the hyperfine-rotational perturbation.

Table 1. Molecular constants (in kHz) within the vibronic ground state of ^{40}K^{87}Rb.

	^{40}K^{87}Rb
$B_{\rm eff}$[a]	1113950(5)[b]/1113952(1)[c]
eQq_1	450[b]
eQq_2	−1410[b]
C_1	−0.0241[d]
C_2	0.4201[d]
C_3	−0.0482[d]
C_4	−2.0304[d]

[a] $B_{\rm eff} = B_0 - 2D_0$, [b] Ref. [27], [c] present study, [d] Ref. [24].

Table 2. Spectral positions (in kHz) and intensities (in arb. units) of the Zeeman-hyperfine spectra in the $J = 1 \leftarrow 0$ transition within the vibronic ground state ($X^1\Sigma$, $v = 0$) of ^{40}K^{87}Rb.

No.	Spectrum		Experimental	Intensity	δ[a]		
	$(\|J',M_J',M_1',M_2'\rangle \leftarrow \|J'',M_J'',M_1'',M_2''\rangle)$				Original		Present
					Uncoupled	Coupled	
1	$\|1,1,-4,1/2\rangle$	$\|0,0,-4,1/2\rangle$	2227837(5)	0.0327	−2	3	1
2	$\|1,0,-4,1/2\rangle$	$\|0,0,-4,1/2\rangle$	2228125(5)	0.0308	−5	3	−2
3	$\|1,-1,-4,1/2\rangle$	$\|0,0,-4,1/2\rangle$	2227774(7)	0.0445	2	5	6
4	$\|1,0,-4,3/2\rangle$	$\|0,0,-4,1/2\rangle$	2227009(2)	0.0039	0	50	4
5	$\|1,-1,-4,3/2\rangle$	$\|0,0,-4,1/2\rangle$	2227133(20)	0.0031	−5	−1	−1
6	$\|1,0,-3,1/2\rangle$	$\|0,0,-4,1/2\rangle$	2228237(10)	0.0088	−12	6	−8
7	$\|1,1,-4,-1/2\rangle$	$\|0,0,-4,1/2\rangle$	2228588(5)	0.0040	5	2	9
8	$\|1,0,-4,1/2\rangle$	$\|0,0,-4,1/2\rangle$	2228804(1)	0.0042	1	−17	5
9	$\|1,0,-4,3/2\rangle$	$\|0,0,-4,3/2\rangle$	2227765(10)	0.0311	−3	48	1
10	$\|1,0,-3,1/2\rangle$[b]	$\|0,0,-3,1/2\rangle$	2228109(16)	0.0157	−17	0	−13
		σ[c]			10.82	20.80	7.92

[a] Deviations from the experimental values: $\delta = \nu_{\rm cal} - \nu_{\rm obs}$, $\delta_{\rm org}$ adopting the original B_0 of Ref. [27], $\delta_{\rm pres}$ adopting the newly refitted $B_{\rm eff}$. [b] Miss-assigned or mistyped as $|1,0,-3,3/2\rangle$ in Ref. [27]. [c] σ is the overall root-mean-square error.

To verify our computer program, the Zeeman-hyperfine-rotational spectra are computed to compare them with the experimental ones[27] (the 4th column and the errors in the brackets are due to the uncertainty of the residual electric field, as denoted in Ref. [27]), which are listed in Table 2. The overall root-mean-square error of 10.82 kHz ($< 10^{-6}$) proves the effectiveness of our methods. Note that the spectrum of $|1,0,-3,1/2\rangle$–$|0,0,-3,1/2\rangle$ was miss-assigned or mistyped as $|1,0,-3,3/2\rangle$–$|0,0,-3,1/2\rangle$ in Ref. [27]. The spectral intensities (the 5th column) in Table 2, which are basically consistent with those of Ref. [25], are calculated based on the transition dipole moments, as expressed in Eqs. (1)–(7) of Ref. [29]. The calculated results in the present study are basically consistent with the experimental values due to the use of the latest molecular constants, and the errors (the 6th column) are listed in Table 2. After having gained insight into the errors, we find that the predictions generally exhibit a negative deviation from the experimental results, as shown by the blue line in Fig. 1. The overall shift should be attributable to the imprecise rotational constant B_0. In addition, the rotational centrifugal distortion constant D_0 is typically 10^{-6} times that of B_0, and thus, D_0 is usually neglected at low-J. However, due to the high precision of B_0 achieved by Ye's group,[27] it is found that D_0 does affect the last digit of B_0 in units of kHz. Unfortunately, since only the experimental Zeeman-hyperfine-spectra for the $J = 1 \leftarrow 0$ transition were available, B_0 and D_0 cannot be fitted simultaneously. Therefore, only the effective rotational constant $B_{\rm eff}$ can be achieved, where $B_{\rm eff} = B_0 - 2D_0$ and is refitted as 1113952(1) kHz (appended to Table 1), and thus, the spectra are recalculated. The blue and red lines in Fig. 1 represent the mean values of the original ($\delta_{\rm org}$) and the present ($\delta_{\rm pres}$) deviations, respectively. The nearly 0 mean de-

viation $\delta_{\rm pres}$ and the low root-mean-square (RMS) error $\sigma_{\rm pres}$ suggest the accuracy of the present $B_{\rm eff}$. The new deviations (the 8th column) and the RMS errors are also listed in Table 2.

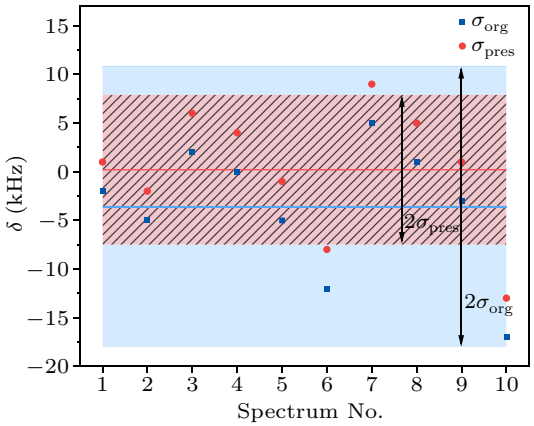


Fig. 1. Errors between the theoretically calculated values under the uncoupled basis set and the experimental values. Blue and red lines, −3.6 kHz and 0.2 kHz, respectively, represent the mean values of $\delta_{\rm org}$ and $\delta_{\rm pres}$. Heights of the blue and red shaded regions represent twice the standard overall deviation $\sigma_{\rm org}$ and $\sigma_{\rm pres}$ of $\delta_{\rm org}$ and $\delta_{\rm pres}$, respectively.

3.2. Hyperfine-rotational structures and perturbation

For closed-shell molecules ($^1\Sigma$) with very weak intramolecular interactions, the hyperfine splitting mainly depends on the presence of nuclear electric quadrupole moments and/or nuclear spin magnetic moments. The electric quadrupole interaction dominates the nuclear hyperfine interaction in the $^1\Sigma$ state except in the $J = 0$ rotational state where it is basically 0 if we neglect the rotational perturbation. Alkali metal diatomic molecules with two non-zero nuclear spins have very rich spin structure, which means that the nuclear spins interact with one another and with the molecular rotation, leading to the splitting of rotational levels. To analyze the complex spectra of alkali metal diatomic molecules, we need to determine the effective Hamiltonian ($H = H_{\rm rot} + H_{\rm hf} = H_{\rm rot} + H_{\rm sr} + H_{\rm ss} + H_{\rm Q}$), as shown in Eq. (2) of Ref. [30]. In the field-free case, the relative error obtained on coupled and uncoupled bases is within 10^{-6}, and the total angular momentum F is a good quantum number. Thus, we deduce the Hamiltonian matrices of KRb on the $|JI_1GI_2F\rangle$ basis employing Wigner–Eckart theory, as expressed by Eqs. (1)–(4), and explore the influence of the perturbation within the same J on the hyperfine levels.

The hyperfine matrix elements of the $J = 1$ hyperfine levels (neglecting the rotational perturbation) are listed in Table 3, and it is of Hermitian conjugate symmetry. The off-diagonal elements represent the hyperfine perturbations. For example, there is a perturbation between the $|G,F\rangle = |3,2.5\rangle$ state and the $|4,2.5\rangle$ state, causing $|3,2.5\rangle$ to shift from 2227847 kHz to 2227971 kHz (absolute shift of 124 kHz and relative shift about 6×10^{-5}) and $|4,2.5\rangle$ to shift from 2227783 kHz to 2227659 kHz. Meanwhile, the $|3,3.5\rangle$ state is co-perturbed by the $|4,3.5\rangle$ and $|5,3.5\rangle$, causing it to shift from 2227797 kHz to 2227606 kHz. Therefore, the pure hyperfine perturbation selection rules can be summarized as $\Delta G = \pm 1, \pm 2$ and $\Delta F = 0$. For the $J = 1$ hyperfine levels, they are not only affected by the pure hyperfine perturbation but also by the rotational perturbation of higher J. For the $J = 0$ hyperfine levels, they do not fulfill the hyperfine perturbation selection rules above, and so the pure hyperfine perturbation is absent and only the rotational perturbation works. Similarly, rotational perturbation selection rules can be obtained by studying the matrix including higher Js. When $\Delta J = \pm 2$ is satisfied, the hyperfine perturbation selection rules of the rotational state are $\Delta G = 0, \pm 1, \pm 2$ and $\Delta F = 0$. Therefore, the hyperfine perturbation selection rules apply when $\Delta J = 0$, $\Delta G = \pm 1, \pm 2$ and $\Delta F = 0$, and when $\Delta J = \pm 2$, $\Delta G = 0, \pm 1, \pm 2$ and $\Delta F = 0$.

Similarly, the effects of electric quadrupole and magnetic dipole moments on the hyperfine levels are discussed as well. Table 4 lists the effects of electric quadrupole interactions, nuclear spin–rotation interactions and nuclear spin–spin interactions on the hyperfine levels of $J = 0$ and 1, respectively. The scalar nuclear spin–spin interaction causes a frequency shift of $-12.2 \sim 15.2$ kHz in the $J = 0$ and 1 rotational levels. For the $J = 0$ rotational level, only the scalar nuclear spin–spin

Table 3. The matrix (in kHz) of the hyperfine levels of the $J = 1$ state in the vibronic ground state of KRb. The matrix is Hermitian, and so the symmetric elements are omitted.

G, F \ G', F'	3, 1.5	3, 2.5	3, 3.5	3, 4.5	4, 2.5	4, 3.5	4, 4.5	4, 5.5	5, 3.5	5, 4.5	5, 5.5	5, 6.5
3, 1.5	2227942	0	0	0	0	0	0	0	0	0	0	0
3, 2.5		2227847	0	0	153	0	0	0	0	0	0	0
3, 3.5			2227797	0	0	61	0	0	206	0	0	0
3, 4.5				2227874	0	0	−120	0	0	261	0	0
4, 2.5					2227783	0	0	0	0	0	0	0
4, 3.5						2228047	0	0	−214	0	0	0
4, 4.5							2228134	0	0	−69	0	0
4, 5.5								2227852	0	0	176	0
5, 3.5									2228013	0	0	0
5, 4.5										2227823	0	0
5, 5.5											2227763	0
5, 6.5												2227936

Table 4. The contribution (in kHz) of various interactions to hyperfine levels of ^{40}K^{87}Rb within its vibronic ground state ($X^1\Sigma$, $v = 0$).

Interaction		$J = 0$	$J = 1$
Nuclear spin–rotation	shift	0	−0.9 ∼0.8
	splitting	0	0.02∼0.34
Tensor nuclear spin–spin	shift	0	−0.24∼0.30
	splitting	0	0.006∼0.14
Scalar nuclear spin–spin	shift	−12.2∼15.2	−12.2∼15.2
	splitting	7.1∼11.2	0.15∼9.80
Nuclear electric quadrupole	shift	$-0.023 \sim -0.015$	−313.7∼360.8
	splitting	$2\times10^{-3} \sim 4\times10^{-3}$	2.8∼279.8

interaction contributes to the hyperfine splitting, and no quadrupole splitting takes place. However, due to the rotational perturbation, the electric quadrupole interactions indirectly cause a frequency shift of about 0.02 kHz. For the hyperfine levels of $J = 1$, the electric quadrupole interactions cause the hyperfine splitting at about −313.7∼360.8 kHz. The nuclear spin–rotation and tensor nuclear spin–spin interactions have the same order influence, both within 10^{-1} kHz. Thus, for the $J = 1$ rotational level, the electric quadrupole interactions play a dominant role in the hyperfine structure.

3.3. Pure hyperfine spectra

The pure hyperfine spectral intensities are derived from the nuclear magnetic dipole transitions. The pure hyperfine spectra within the rovibronic ground state ($X^1\Sigma$, $v = 0$, $J = 0$) of the ^{40}K^{87}Rb are plotted in Fig. 2, and the inset illustrates the hyperfine levels. Note that the spectral natural linewidth is much smaller due to the weak magnetic transition probability, and thus, the simulated spectral linewidth is dominated by the RF excitation source of about 7 Hz.

The hyperfine levels, as illustrated in the inset in Fig. 2, can be expressed using the nuclear spins and the scalar nuclear spin–spin interaction constant as

$$E_{2.5} = -(I_1I_2 + I_2) \times C_4 = -C_4 \times 15/2, \quad (7)$$

$$E_{3.5} = -(I_1I_2 - I_1 + 2I_2 - 1) \times C_4 = -C_4 \times 4, \quad (8)$$

$$E_{4.5} = -(I_1I_2 - 2I_1 + 3I_2 - 3) \times C_4 = C_4 \times 1/2, \quad (9)$$

$$E_{5.5} = I_1I_2 \times C_4 = C_4 \times 6. \quad (10)$$

Thus, the pure hyperfine spectral positions are only determined by C_4. Therefore, the scalar nuclear spin–spin interaction constant C_4 can be precisely determined by pure hyperfine spectral investigation.

The pure hyperfine spectra within $J = 1$ in the vibronic ground state ($X^1\Sigma$, $v = 0$) of the ^{40}K^{87}Rb are plotted in Fig. 3. The transition selection rules are summarized as $\Delta G = 0$ and $\Delta F = 1$. The (#) numbered spectra are too weak to observe and not plotted, but are listed in supplementary Table 1. Although the spectral positions are dominated by the nuclear electric quadrupole interactions, they are also slightly shifted by the scalar and tensor nuclear spin–spin interactions, as listed in Table 4. Therefore, when the nuclear electric quadrupole interaction constants are determined by the hyperfine-rotational spectroscopy[27] and the scalar nuclear spin–spin interaction constant is determined by the pure hyperfine spectroscopy within the $J = 0$ state (as discussed in the above subsection), the tensor nuclear spin–spin interaction constant can be precisely determined by the pure hyperfine spectroscopy within the $J = 1$ state. This means that the scalar and tensor nuclear spin–spin interaction constants can be determined by the pure hyperfine spectroscopy.

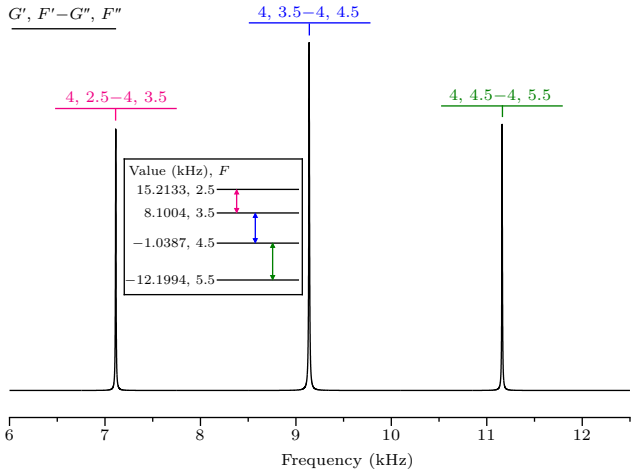


Fig. 2. Simulated pure hyperfine spectra within the rovibronic ground state ($X^1\Sigma$, $v = 0$, $J = 0$) of ^{40}K^{87}Rb, and the inset illustrates the hyperfine levels. Quantum numbers of the two states of the pure hyperfine spectra are labeled, and the colors correspond to the colors of the arrows in the inset. Simulated spectral linewidth is dominated by the RF excitation source of about 7 Hz.

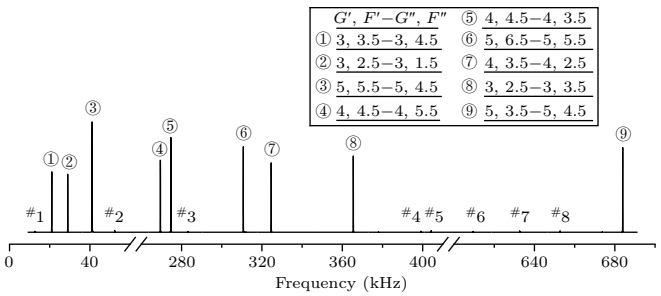


Fig. 3. Simulated pure hyperfine spectra in $J = 1$ within the vibronic ground state of ^{40}K^{87}Rb, and quantum numbers of the two states involved are also labeled. Intensities of the spectra marked with letters (such as $^{\#}1$, $^{\#}2$, $^{\#}3$,…) are about two orders of magnitude smaller than those of the spectra marked with numbers (such as ①, ②, ③,…). At the same sensitivity, these weaker spectral lines are difficult to observe.

4. Conclusion

The Zeeman-hyperfine-rotational spectra of ^{40}K^{87}Rb in its vibronic ground state are theoretically studied and are in good agreement with the experimental ones, and the newly fitted $B_{\rm eff} = 1113952(1)$ kHz reduces the overall deviation from 10.82 kHz to 7.92 kHz. Thereafter, the pure hyperfine spectra within the $J = 0$ and 1 rotational states are simulated, and

the transition selection rules are summarized as $\Delta G = 0$ and $\Delta F = 1$. The perturbations are discussed in detail to precisely determine the spectral positions, and the perturbation selection rules are summarized as when $\Delta J = 0$, $\Delta G = \pm 1, \pm 2$ and $\Delta F = 0$, and when $\Delta J = \pm 2$, $\Delta G = 0, \pm 1, \pm 2$ and $\Delta F = 0$. For $J = 0$, the pure hyperfine spectral positions are only determined by the scalar nuclear spin–spin interaction, while for $J = 1$, the pure hyperfine spectral positions are also affected by the tensor nuclear spin–spin interaction. Therefore, the nuclear spin–spin interaction constants can be precisely determined by the pure hyperfine spectroscopy. Furthermore, the study of pure hyperfine spectroscopy provides a certain possibility to realize quantum computation by RF manipulation.[25,26]

Acknowledgments

Project supported by the National Natural Science Foundation of China (Grant No. 12004199). We also gratefully acknowledge Professor Martin W. Zwierlein from MIT Harvard Center Ultracold Atoms and Professor Jeremy M. Huston from Durham University for the discussion on hyperfine interactions.

References

[1] Hughes M, Frye M D, Sawant R, Bhole G, Jones J A, Cornish S L, Tarbutt M R, Hutson J M, Jaksch D and Mur-Petit J 2020 *Phys. Rev. A* **101** 062308
[2] DeMille D 2002 *Phys. Rev. Lett.* **88** 067901
[3] Yelin S F, Kirby K and Côté R 2006 *Phys. Rev. A* **74** 050301
[4] McDonald M, McGuyer B H, Apfelbeck F, Lee C H, Majewska I, Moszynski R and Zelevinsky T 2016 *Nature* **535** 122
[5] Hudson E R, Lewandowski H J, Sawyer B C and Ye J 2006 *Phys. Rev. Lett.* **96** 143004
[6] DeMille D, Doyle J M and Sushkov A O 2017 *Science* **357** 990
[7] Shuman E S, Barry J F and Demille D 2010 *Nature* **467** 820
[8] Ding S Q, Wu Y W, Finneran I A, Burau J J and Ye J 2020 *Phys. Rev. X* **10** 021049
[9] Zhelyazkova V, Cournol A, Wall T E, Matsushima A, Hudson J J, Hinds E A, Tarbutt M R and Sauer B E 2014 *Phys. Rev. A* **89** 053416
[10] Zhang Y H, Zeng Z X, Liang Q, Bu W H and Yan B 2022 *Phys. Rev. A* **105** 033307
[11] Ni K K, Ospelkaus S, de Miranda M H, Pe'er A, Neyenhuis B, Zirbel J J, Kotochigova S, Julienne P S, Jin D S and Ye J 2008 *Science* **322** 231
[12] Molony P K, Gregory P D, Ji Z H, Lu B, Köppinger M P, Le Sueur C R, Blackley C L, Hutson J M and Cornish S L 2014 *Phys. Rev. Lett.* **113** 255301
[13] Guo M, Zhu B, Lu B, Ye X, Wang F, Vexiau R, Bouloufa-Maafa N, Quemener G, Dulieu O and Wang D 2016 *Phys. Rev. Lett.* **116** 205303
[14] Liu W, Wu J, Ma J, Li P, Sovkov V B, Xiao L and Jia S 2016 *Phys. Rev. A* **94** 032518
[15] Wu J, Liu W, Wang X, Ma J, Li D, Sovkov V B, Xiao L and Jia S 2018 *J. Chem. Phys.* **148** 174304
[16] Yang H, Zhang D C, Liu L, Liu Y X, Nan J, Zhao B and Pan J W 2019 *Science* **363** 261
[17] De Marco L, Valtolina G, Matsuda K, Tobias W G, Covey J P and Ye J 2019 *Science* **363** 853
[18] Duda M, Chen X Y, Schindewolf A, Bause R, von Milczewski J, Schmidt R, Bloch I and Luo X Y 2023 *Nat. Phys.* **19** 720
[19] Bigagli N, Yuan W J, Zhang S W, Bulatovic B, Karman T, Stevenson I and Will S 2024 *Nature* **631** 289
[20] Hudson J J, Kara D M, Smallman I J, Sauer B E, Tarbutt M R and Hinds E A 2011 *Nature* **473** 493
[21] Tarbutt M R, Sauer B E, Hudson J J and Hinds E A 2013 *New J. Phys.* **15** 053034
[22] Parker R H, Yu C H, Zhong W C, Estey B and Müller H 2018 *Science* **360** 191
[23] Turro N J 1983 *Proc. Natl. Acad. Sci. USA* **80** 609
[24] Aldegunde J, Rivington B A, Żuchowski P S and Hutson J M 2008 *Phys. Rev. A* **78** 033434
[25] Aldegunde J, Ran H and Hutson J M 2009 *Phys. Rev. A* **80** 043410
[26] Ran H, Aldegunde J and Hutson J M 2010 *New J. Phys.* **12** 043015
[27] Ospelkaus S, Ni K K, Quéméner G, Neyenhuis B, Wang D, de Miranda M H, Bohn J L, Ye J and Jin D S 2010 *Phys. Rev. Lett.* **104** 030402
[28] Wang D F, Shao X P, Huang Y X, Li C L and Yang X H 2021 *Chin. Phys. B* **30** 113301
[29] Ouyang Q, Chen R, Shao X P, Huang Y X and Yang X H 2025 *Int. J. Mod. Phys. B*
[30] Chen R, Shao X P, Huang Y X and Yang X H 2023 *Acta Phys. Sin.* **72** 043301 (in Chinese)